Molecular-dynamics study of orientational order in liquids and glasses and its relation to the glass transition

T. Tomida
Advanced Technology Research Laboratories, Sumitomo Metal Industries, Ltd., 1-8 Fusocho, Amagasaki 660, Japan

T. Egami
Department of Materials Science and Engineering and Laboratory for Research on the Structure of Matter, University of Pennsylvania, Philadelphia, Pennsylvania 19104-6272

(Received 27 June 1994; revised manuscript received 21 February 1995)

Molecular-dynamics simulations of monatomic liquids interacting via a modified Johnson potential have been carried out to investigate the structure of liquids and the microscopic mechanism of the glass transition. The structure of liquids is described in terms of spherical harmonic representations of topology of local clusters and the orientational correlation among them. The variation of the averaged topology of the nearest-neighbor clusters exhibits an anomalous behavior at temperatures between the glass transition temperature (T_g) and a temperature much above T_g. This anomalous behavior is shown to be caused by aggregation of the clusters with icosahedral topology. The number of the icosahedral clusters increases progressively with decreasing temperature, and, at T_g, the increase is abruptly arrested. Within the icosahedral aggregates, the strong mirror-related orientational correlation exists with a correlation length growing over 10 Å near the glass transition temperature. The percolation of the icosahedral clusters and the mirror-related orientational order leading to the glass transition are discussed.

I. INTRODUCTION

Despite numerous experimental and theoretical attempts to determine the structural nature of liquids and glasses, no satisfactory understanding has been attained because of the complexity of the structure lacking translational symmetry. This unsatisfactory state of affairs has impeded not only the description of the properties of glasses from an atomistic point of view, but also clarification of the mechanism of the glass transition. The purpose of this work is to introduce a concept of successively mirrored orientational correlation due to interlocking icosahedral clusters and to attempt to describe some novel aspects of the orientational order in supercooled liquids and its relation to the mechanism of the glass transition via molecular dynamics (MD).

Glassy structures are often described as resulting from the competition between packing of tetrahedra maximizing local packing density and the frustration imposed by topological and geometrical rules to attain global space filling.[1–5] The space cannot be filled by regular tetrahedra alone, though the tetrahedral arrangement of atoms achieves the densest local packing. Abundant results mainly from model structure building[6–9] support this view of the glassy structure. The presence of tetrahedral packing was first noted by Frank[10] 40 years ago. Frank pointed out that at zero temperature a Lennard-Jones particle and its 12 nearest neighbors prefer to form an icosahedron that consists of 20 slightly distorted tetrahedra; the icosahedral arrangement has a significantly higher binding energy than the 13-atom cluster which forms the crystalline close-packed structure. Therefore a relevant question to ask in trying to characterize the structure of liquids and glasses is how the tetrahedra are spatially correlated to each other in the structure. Two important approaches to this question have been introduced by Steinhardt, Nelson, and Ronchetti,[11] and by Kléman and Sadoc.[1–3]

Steinhardt, Nelson, and Ronchetti[11] studied the orientational correlation between bonds defined by nearest-neighbor atoms in model glasses constructed via MD using a Lennard-Jones potential. In this simulation, a long-range bond orientational order was identified at a temperature 20% below the empirical freezing temperature for the Lennard-Jones system. Furthermore, in agreement with the prediction by Frank,[10] the order was found to possess an icosahedral symmetry. Although their MD results concerning the long-range icosahedral order are controversial,[12] the way they have proposed to analyze the orientational correlation provides valuable insight into the study of the order in condensed matter, which has actually led to the novel idea of icosahedral quasicrystals.

On the other hand, Kléman and Sadoc[1–3] started their thought-provoking approach in a curved space. The curved space, which is a surface of a sphere in four dimensions, can be tiled completely by tetrahedra alone, therefore by icosahedra, if it has the right curvature. The complete icosahedral packing is then mapped onto ordinary flat space by introducing minimal disclination-line defects. The introduced disclination network creates strain fields in the icosahedral packing and fits them in the flat space. The obtained structure, however, depends upon the mapping process, and details of the disclination networks to reproduce realistic glassy structures are not

known. Nevertheless, this conceptual and geometrical model implies that local clusters with an icosahedral symmetry could aggregate in the structure of glasses until the disclination intervenes to reduce the geometrical frustration caused by the aggregation, and a certain orientational order provoked by the aggregation could develop in the structure.

Such a "hidden" order in glassy structures has also been argued for many years in connection with one of the most formidable problems in condensed-matter science: whether the glass transition is kinetic or thermodynamic. The kinetic nature of the glass transition is clearly seen in the cooling-rate dependence of glass transition temperatures.[13] The glass transition temperature (T_g), as defined by a discontinuous change in heat capacity, is displaced to a lower temperature by a decrease of cooling rates; if there is no lower limit of the transition temperature, the transition is purely kinetic. However, as Kauzmann[14] pointed out about 50 years ago, an extrapolation of the configurational entropy of various glass formers to lower temperatures indicates the presence of a lower bound of T_g.[14,15] This suggestion is indeed supported by a recent calorimetric measurement made by Brüning and Samwer.[16] Their results by an extended calorimetric measurement on several glass-forming systems suggest that T_g and the temperature width of the transition may decouple from experimental time scales for sufficiently slow heating rates. Other experiments, for example, on atomic vibrations[17] also imply some collective phenomena underlying the transition.

Much of the theoretical effort on the glass transition has also been directed to dynamical explanations of freezing. A polymer-configuration model by Gibbs and coworkers[18,19] and a free-volume model by Cohen and coworkers[20–22] assume underlying equilibrium transitions to ideal glassy structures, which never is practically obtainable because of intervening kinetic freezing. The mode-coupling theory developed by several groups[23–26] treats the glass transition as a purely thermodynamical one. The first two theories deal with mixing or communal entropies, and the last incorporates nonlinear terms involving hydrodynamic viscosity. On the other hand, Saslow[27] presented recently a Landau theory to derive the well-known Vogel-Tamman-Fulcher (VTF) law[28] for the slowing down of relaxation processes. In this theory, a global ordering that is frustrated by a quenched-in randomness or a local order incompatible with the global order and an Arrhenius-type relaxation process of local regions toward the global order are assumed. The barrier height for the relaxation is then shown to vary as $(T-T_0)^{-1}$ in a wide temperature range, resulting in the VTF law. As connoted by the author,[27] this Landau theory of the glass transition may be related to the above-mentioned work concerning the icosahedral orientational order that is incompatible with the crystalline translational one.

In this paper, we start by retracing the way to describe the orientational order in glasses introduced by Steinhardt, Nelson, and Ronchetti[11] and then extend the idea to analyze the topology of local clusters defined as a "cage" of nearest neighbors and the orientational correlation among them. Based on this extended concept, geometrical properties and their temperature dependence of model supercooled liquids constructed by MD using a modified Johnson potential[29] are then investigated. The temperature dependence of the symmetry parameters of the local clusters indicates the presence of another transition temperature much above T_g. This second transition temperature and T_g are shown to relate to aggregation of the clusters with an icosahedral topology and the two types of percolation among the aggregates. It is further shown here that strong orientational correlation with mirror reflection exists within the icosahedral aggregates. The energetics of the icosahedral clusters, leading to aggregation of the clusters in liquids, and the relation of the percolation and the mirror-related orientational correlation to the glass transition are discussed.

II. MATHEMATICAL EXPRESSIONS OF ORIENTATIONAL ORDERS

A. Bond orientational correlation functions

We first reintroduce the way Steinhardt, Nelson, and Ronchetti[11] have proposed to analyze bond orientational order (BOO) in glasses and then extend the idea to describe the orientational correlation among the clusters defined as sets of atoms which are near neighbors to each other.

To study BOO, Steinhardt, Nelson, and Ronchetti have defined a set of "bonds" joining an atom to its nearest neighbors and the spherical harmonics associated with the bond orientation relative to the fixed coordinates as

$$Q_l^m(\vec{r}_\nu)=Y_l^m(\theta(\vec{r}_\nu),\phi(\vec{r}_\nu)) , \tag{1}$$

where the vector $\vec{r}_\nu$ represents the midpoint of the νth bond, θ and ϕ refer to the angle between the bond and the coordinates, and Y_l^m denotes the spherical harmonic functions. Using Q_l^m, they define the bond orientational correlation function $G_l(r)$,

$$G_l(r)=\frac{1}{2l+1}\frac{\sum_m\sum_{\nu,\mu}Q_l^m(\vec{r}_\nu)Q^{*m}_l(\vec{r}_\mu)\delta(|\vec{r}_\nu-\vec{r}_\mu|-r)}{\sum_{\nu,\mu}Q_0^0(\vec{r}_\nu)Q^{*0}_0(\vec{r}_\mu)\delta(|\vec{r}_\nu-\vec{r}_\mu|-r)} , \tag{2}$$

where r denotes the distance between the bonds. When there exists, for instance, an icosahedral type of long-range BOO such as those in icosahedral quasicrystals, the functions with l being more than 6, e.g., G_6 and G_{10}, signal it by being nondecaying functions.

B. Cluster orientational correlation functions and cluster symmetry coefficients

Alternatively, however, we may choose to evaluate the angular correlation between local clusters than just the angular correlation between the bonds. The reason for this will be clarified later. Here the local cluster is defined simply as a polyhedron consisting of an atom at the center and the nearest-neighbor atoms occupying its

vertices. Note that the number of clusters defined in a system is equal to that of the atoms involved, since these clusters are allowed to overlap each other. The orientation and geometry of the cluster can be evaluated by summing up the spherical harmonics associated with the bonds connecting the center atom of a cluster to the atoms at its vertices, $q_l{}^m$,

$$q_l{}^m(\vec{r}_i)=\sum_{\substack{j \\ \text{nearest} \\ \text{to the } i\text{th}}} Y_l{}^m\left[\frac{\vec{r}_i-\vec{r}_j}{|\vec{r}_i-\vec{r}_j|}\right] . \tag{3}$$

The vectors $\vec{r}_i$ and $\vec{r}_j$ in this equation represent the positions of the center atom and its nearest-neighbor atoms, hence the vertices, respectively. The difference between the bonds and clusters defined here is illustrated in Fig. 1.

Furthermore, defining the position of a cluster by that of its central atom, a cluster orientational correlation function can be defined as

$$J_l(r)=\frac{1}{2l+1}\frac{\sum_m\sum_{i,j}q_l{}^m(\vec{r}_i)q^{*m}_l(\vec{r}_j)\delta(|\vec{r}_i-\vec{r}_j|-r)}{\sum_{i,j}q_0{}^0(\vec{r}_i)q^{*0}_0(\vec{r}_j)\delta(|\vec{r}_i-\vec{r}_j|-r)} , \tag{4}$$

where r denotes the length of a "cluster bond" connecting center atoms of two clusters instead of the bond distance unlike in $G_l(r)$. This function, as well as $G_l(r)$, is invariant under the rotation of external coordinates.

This function provides information concerning not only the orientational correlation in the system, but also the averaged geometry of the clusters by its value evaluated at r being zero, $\hat{J}_l$,

$$\hat{J}_l=J_l(r=0)=\frac{1}{2l+1}\frac{\sum_i\sum_m|q_l{}^m(\vec{r}_i)|^2}{\sum_i|q_0{}^0(\vec{r}_i)|^2} . \tag{5}$$

$\hat{J}_l$ is approximately equivalent to the cluster average of the following spherical harmonics associated with each local cluster:

$$\hat{J}_l\simeq\left\langle\hat{J}_{cl}=\frac{1}{2l+1}\frac{\sum_m|q_l{}^m|^2}{|q_0{}^0|^2}\right\rangle_{\text{cluster average}} . \tag{6}$$

Note that $\hat{J}_l$ is exactly the same as the cluster average if the number of atoms included in each cluster is the same.

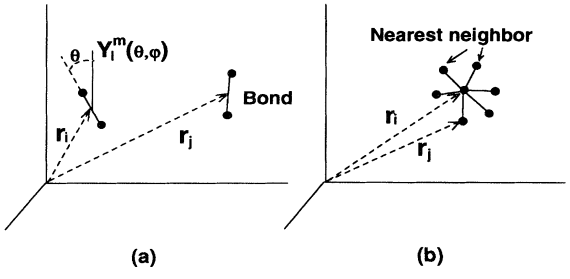

FIG. 1. Schematic representation of (a) bond-angle correlation calculation and (b) cluster-angle correlation calculation.

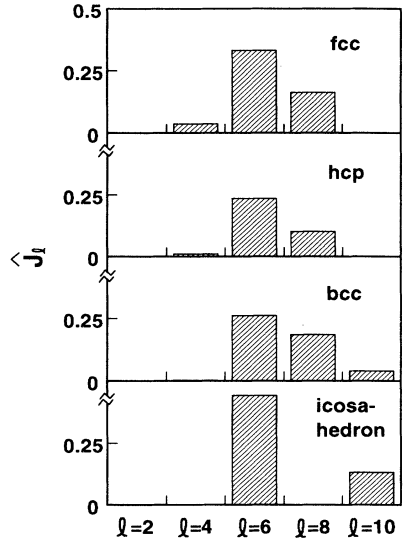

FIG. 2. $\hat{J}_l$'s calculated for fcc, hcp, bcc, and icosahedral clusters.

It is instructive to calculate the symmetry parameters $\hat{J}_l$'s for clusters with simple geometries. The calculated values for fcc, hcp, bcc, and icosahedral clusters are shown in Fig. 2. These fcc, hcp, and icosahedral clusters consist of 13 atoms including an atom at the center of each cluster, and the bcc cluster consists of 15 atoms including the second-nearest-neighbor atoms as well as the first-nearest neighbors and the central atom. These parameters show a dramatic variation among the clusters. For the fcc, hcp, and bcc clusters, the fourth-order parameter $\hat{J}_4$ is the nonzero parameter of the lowest order except for the zeroth order. However, when the cluster is an icosahedron, the parameters with l being 2, 4, and 8 are zero, and the parameters with l being 6 and 10 show the largest values among the clusters. These trends are very similar to those of the bond orientational correlation parameter Q_l after Steinhardt, Nelson, and Ronchetti.[11] Indeed, for such simple clusters, $\hat{J}_l$ is exactly the square of Q_l. The primary difference between $\hat{J}_l$ and Q_l is that $\hat{J}_l$ does not depend on the orientational correlation between clusters when the evaluation is extended for a system consisting of many clusters, whereas Q_l does depend and vanishes if the clusters are uncorrelated. In other words, $\hat{J}_l$ is purely a parameter of local geometry, while Q_l is a measure of global correlation.

C. Mirror-related orientational correlation functions

Although icosahedral clusters cannot fill space by themselves, one might imagine that the icosahedral clusters aggregate in an orderly fashion, until structural frustration produced by aggregation builds up to suppress aggregation itself. Two of the simplest connections or interlocking states between two icosahedral clusters are shown in Figs. 3(a) and 3(b), which could be a unit of ag-

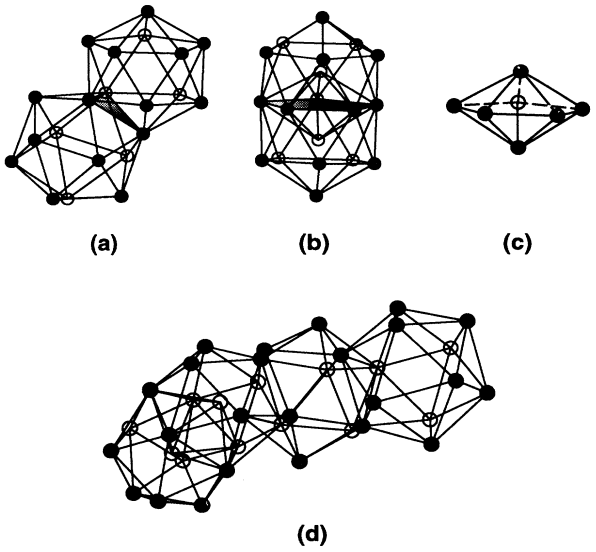

FIG. 3. (a),(b) Two simple interlocking states of icosahedral clusters, (c) a pentagonal bipiramid, and (d) an ideal aggregation of four icosahedral clusters interconnected in a manner shown in (a) and (b).

gregation. One is by sharing a triangle face, therefore sharing three nearest-neighbor atoms. The other is the interconnection where one of the vertices of a cluster lies on the center of the other cluster, and the clusters share a pentagonal bipiramid or a heptatope cluster shown in Fig. 3(c). The latter requires about 10% dilatation of icosahedra in the direction of the bond connecting the two cluster centers, while the former does not. Note that one of the two interlocking icosahedral clusters in either case cannot be superimposed on the other by translation, but they are related by mirror symmetry.

So as to understand how such icosahedral aggregations are reflected in the orientational correlation, functions $J_6(r)$ and $J_{10}(r)$ have been calculated for the above simple cases. In this calculation, we neglect the dilatation of the icosahedra required for the aggregation shown in Fig. 3(b). Moreover, fractional coordinates are used so that the cluster distances are measured in units of the distance between the center and a vertex of the icosahedra; i.e., the distance between the two icosahedra shown in Fig. 3(b) is the unit. The results are shown in Table I. This reveals that the values of the sixth-order function are negative for both cases, while that of the tenth-order function changes its sign depending on the type of the aggregation, therefore the cluster distance. It is noteworthy that not only $J_l(r)$, but also $G_l(r)$ responds to these icosahedral aggregations in this fashion. Therefore, as this type of the orientational correlation develops in glasses, the sign of these orientational correlation functions would change with respect to the interbond or intercluster distance, and the positive and negative values could cancel each other at large distances, resulting in an attenuating behavior of the function. The oscillation and attenuation of the orientational correlation can explain the MD results by Ernst and Nagel.[12]

TABLE I. $J_6(r)$ and $J_{10}(r)$ calculated for the interlocking icosahedral clusters shown in Fig. 3.

Intercluster distance r	1 [Fig. 3(b)]	1.304 [Fig. 3(a)]
$J_6(r)$	−0.0529	−0.1178
$J_{10}(r)$	−0.0439	0.0348

The orientational correlation of the aggregated icosahedral clusters can be described without the above-mentioned oscillatory behavior by modifying the definition of $J_l(r)$ by using a mirror or reflection operator. In both of the simple interconnection cases shown in Fig. 3, the two interconnected icosahedra are related by mirror symmetry as mentioned before. For instance, in an aggregate of four icosahedral clusters connected in this fashion, as shown in Fig. 3(d), the orientation of the icosahedron at one end of the aggregation becomes the same as that of the icosahedron at the other end when the structure is reflected 3 times along the three cluster bonds lying in the aggregate in the order of the bonds. Let us define the operator $R(\vec{r})$ to reverse coordinates along the direction of the vector $\vec{r}$ (reflection-symmetric operation against the plane perpendicular to the vector), and R_{ij} to be $R(\vec{r}_i-\vec{r}_j)$. With this reflection operator, the following cluster orientational correlation function can be defined:

$$K_l(r)=\frac{1}{2l+1}\frac{\sum_m \sum_{i,j} q_l{}^m(\vec{r}_i)R_{is}R_{st}\cdots R_{uv}R_{vj}q^{*m}_l(\vec{r}_j)\delta(|\vec{r}_i-\vec{r}_j|-r)}{\sum_{i,j} q_0{}^0(\vec{r}_i)q^{*0}_0(\vec{r}_j)\delta(|\vec{r}_i-\vec{r}_j|-r)}, \tag{7}$$

where sth, tth, . . . , uth, and vth clusters are the ones lying on the connection path between the ith and jth clusters in the order of $i\to s\to t\cdots u\to v\to j$, and $R_{is},R_{st},\ldots,R_{uv}$ or R_{vj} operate on the coordinates of the jth clusters to be mirrored. If these clusters are complete icosahedra and the orientational relation between neighboring clusters is described by mirror symmetry, the magnitude of $K_l(r)$ is of the order of unity. Thus it allows us to analyze if mirror symmetry or orientational anticorrelation exists between the neighboring clusters or

TABLE II. Some properties of the modified Johnson potential (Ref. 29).

Position of the minimum:	2.617 Å
Depth of the minimum:	−0.252 eV
Curvature at the minimum:	1.915 eV/Å^2
Cutoff distance:	3.44 Å

not and, if any, how far such an orientational correlation extends in the glasses without the difficulty due to the oscillatory behavior that characterizes $J_l(r)$ and $G_l(r)$.

III. SIMULATION PROCEDURE

Employing the modified Johnson potential[29] (see the Appendix) that was originally developed for bcc iron,[30] model structures consisting of 1024 or 4394 particles were constructed by MD. This potential is a short-range potential known to reproduce many of the properties of bcc iron.[29,30] Relevant characteristics of the potential are listed in Table II. The integration time step was taken to be 10^{-15} sec, which is about 100th of Debye time of this potential. Periodic boundary conditions were maintained on all six faces of the cubic assembly, and the computation was carried out in a constant-volume mode.

The assembly of 1024 or 4394 particles in a cubic block was first equilibrated in a liquid state for 10^4 time steps at 3000 K. The pressure of the systems during this procedure was maintained at 0.02 eV Å^{-3} by changing the size of the cubic block and linearly displacing all the atoms every 100 time steps, thus using a pseudo-constant-pressure mode.

Two types of cooling procedures were used to construct model structures at various temperatures. In a cooling procedure (process I), the assembly equilibrated at 3000 K was quenched at a rate of 10^{15} K sec^{-1} and then relaxed for 10^4 MD steps at 500 K; both processes were computed in the pseudo-constant-pressure mode so that the pressures of the system during the quench and relaxation processes were maintained at 0.02 eV Å^{-3} and zero, respectively. Subsequently, after switching the MD mode back to a pure constant-volume one, the assembly was heated or cooled to temperatures ranging from 300 to 3000 K at a rate of 10^{16} K sec^{-1}, and the assembly was again relaxed at each temperature for 2×10^4 MD steps in the constant-volume mode. On the other hand, in the other quench procedure (process II), the volume of the system equilibrated at 3000 K was first reduced to increase the density by using the pseudo-constant-pressure algorithm, and the system was eventually cooled at a rate of 10^{15} or 10^{14} K sec^{-1} in the constant-volume mode. The data on five MD runs of which results are presented here are listed in Table III. Furthermore, to investigate the structural relaxation at low temperatures, relatively long relaxation processes up to 6×10^5 MD steps in the constant-volume mode were added to runs C, D, and E. Typical examples of pair distribution functions of the model structures are shown in Fig. 4. Note that there is no indication of crystallization in the model structures.

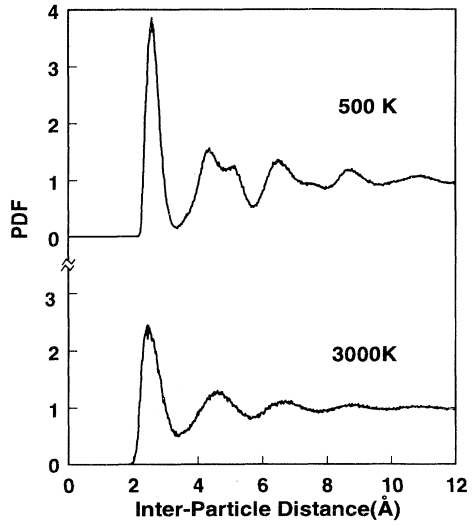

FIG. 4. Pair distribution functions of the model structures at 500 and 3000 K (run A).

Using these model structures, the cluster symmetry coefficients and orientational correlation functions described previously were evaluated. The atomic bonds and local clusters relevant to the evaluations were defined to be bonds connecting the nearest neighbors and the clusters consisting of a particle and its nearest neighbors, respectively. The nearest neighbors to a particle were defined as the ones within an interparticle distance of less than 3.3 Å. This nearest-neighbor definition ensures the neighbors to be within the first peak of their pair distribution function. Evaluations were performed for the atomic positions averaged over 600 time steps rather than in-

TABLE III. Data on the MD runs.

Run	No. of atoms	Density (Å^{-3})	Quenching rate (K/MD step)	Heating rate (K/MD step)	Process
A	1024	0.074 02	1.0	10	I
B	1024	0.074 02	0.1		II
C	1024	0.074 02	1.0		II
D	4394	0.074 62	0.1		II
E	4394	0.078 43	0.1		II

stantaneous positions, unless mentioned otherwise, to eliminate the effects of thermal vibration of atoms. Moreover, for the smaller systems of 1024 particles, the evaluations were repeated 10 times and were averaged to reduce the statistical error.

IV. RESULTS

A. Glass transition temperature

The temperature dependence of the pressure of the systems is shown in Fig. 5. The results of runs B and C are very similar to that of run D and are not shown in the figure. When temperature is lowered from above the experimental melting temperature (1808 K), the pressure decreases almost linearly, suggesting that the system is supercooled without crytallization. However, this temperature dependence clearly starts departing from linearity at around 900 K. We interpret this departure to indicate the glass transition and tentatively call this temperature T_g. This temperature is in good agreement with the T_g reported by Chen, Egami, and Vitek[31] for a system using the same potential and is slightly higher than the experimental T_g's for Fe-based glass-forming alloys (700–800 K).[32] The higher pressure above T_g for run E is, of course, due to the higher density of the system. Furthermore, large deviation of the pressure from linearity below T_g and a somewhat higher transition temperature for run A are likely to be due to the mixed process used for this particular run, consisting of quenching in pseudo-constant pressure and subsequent heating and annealing in constant volume (see Sec. III).

A similar clearly definable slope change also occurs at T_g in the temperature dependence of the total energy, the sum of kinetic and potential energies, as shown in Fig. 6. In addition to this abrupt change at T_g, it is observed that the slope of the total energy variation gradually decreases when increasing the temperature from T_g to above, resulting in a slight but visible convex curvature of the variation. The abrupt slope change at T_g corresponds to a change of the specific heat by about Nk_B, where N is the number of atoms and k_B is Boltzmann's constant, and the gradual slope decrement above T_g yields the specific heat decrease of about $2Nk_B/3$ when the temperature is increased from T_g to 3000 K.

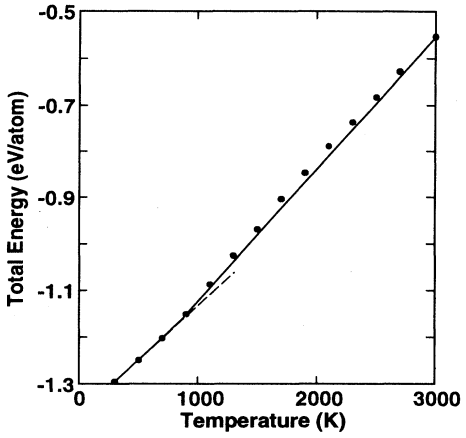

FIG. 6. Temperature dependence of the total energy for run A.

B. Bond orientational order [$G_l(r)$ and $J_l(r)$]

First, we evaluated the bond orientational correlation function $G_6(r)$ by using the instantaneous atomic positions of the model structures. The results are shown in Fig. 7. The correlation function is largely oscillatory and attenuates quickly at large interbond distances both at 500 and 3000 K. Although the attenuation is somewhat slower at 500 K than at 3000 K, no sign of correlation exists beyond the distance of 10 Å at either temperature.

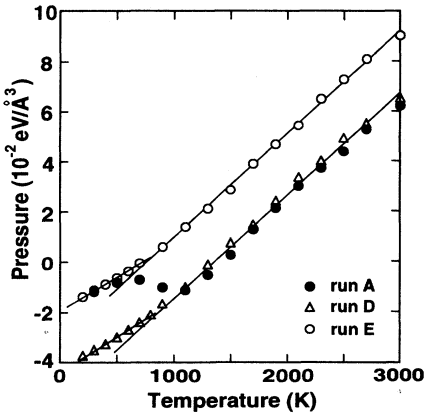

FIG. 5. Temperature dependence of the pressure of model structures.

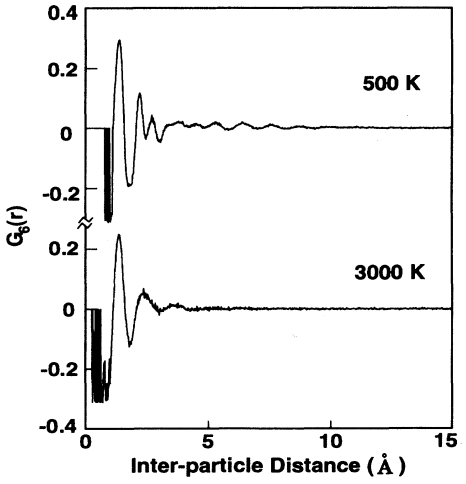

FIG. 7. Bond orientational correlation functions calculated for model structures (run A).

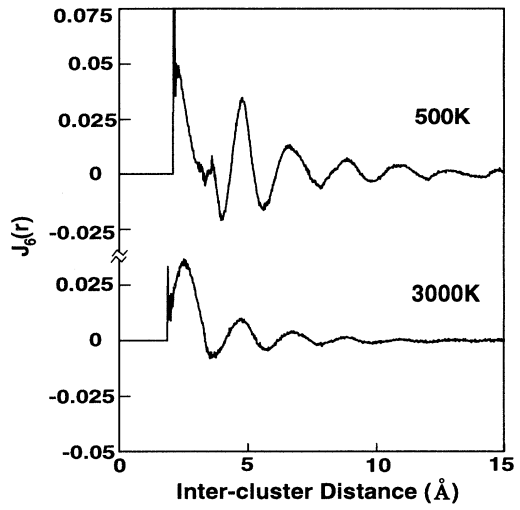

FIG. 8. Cluster orientational correlation functions calculated for model structures (run A).

These trends are in good accordance with previous results using the Lennard-Jones potential,[12] and no indication of the long-range icosahedral BOO reported by Steinhardt, Nelson, and Ronchetti[11] exists in the present result.

As expected by the similarity between $G_l(r)$ and $J_l(r)$, the $J_6(r)$ evaluated for the instantaneous atomic positions also exhibits an oscillatory and attenuating behavior, as shown in Fig. 8. Although the attenuation at a large distance in the $J_6(r)$ is slower than in the $G_6(r)$, the sign of the function changes when increasing the cluster distance quite similarly to that in $G_6(r)$. These results suggest that the oscillatory behavior in these orientational correlation functions is an intrinsic characteristic of the glassy structure, and this could be in part due to the anticorrelation or the mirror relationship among the local clusters mentioned previously.

C. Topology of local clusters and mirror-related orientational order below T_g

1. *Topology of local clusters*

The topology of the local cluster defined as a polyhedron consisting of a center atom and its nearest neighbors on the vertices was analyzed in terms of the parameter $\hat{J}_l$. Figure 9 shows the $\hat{J}_l$'s calculated for the model glass at 700 K. Comparison between these parameters and the $\hat{J}_l$'s calculated for the simple clusters shown in Fig. 2 indicates that the averaged geometry of the clusters is somewhat closer to that of an icosahedron than those of cubic and hcp clusters; the $l=8$ component for the model glass is smaller than those of cubic and hcp clusters, while the $l=10$ component is larger.

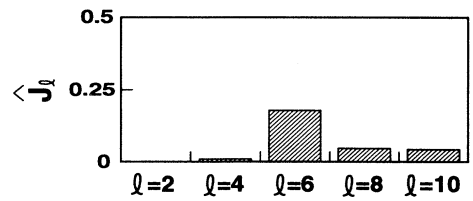

FIG. 9. $\hat{J}_l$'s calculated for the model structure at 700 K (run D).

To evaluate this point further, $\hat{J}_l$ for each cluster, therefore $\hat{J}c_l$ in Eq. (6), was calculated. The distribution of the above parameter among the clusters is shown in Fig. 10. It is quite interesting to note that there seem to be two peaks in the distribution of the $l=6$ component, whereas the $l=4$ and $l=8$ components exhibit simple higher-dimensional Gaussian-type distributions. In the distribution of the $l=6$ component, the larger peak lies around the parameter value of 0.19. The smaller peak, which is somewhat like a shoulder of the larger peak, exists around the parameter value of 0.35 and ends at 0.44. Note that the value of 0.44 happens to correspond to that of $\hat{J}c_6$ for icosahedra, and no cluster exists having a value beyond 0.44. Thus $\hat{J}c_6$ for a perfect icosahedron, 0.44, could be the global maximum of this geometry parameter. Furthermore, the mean $\hat{J}c_6$ value of the smaller peak

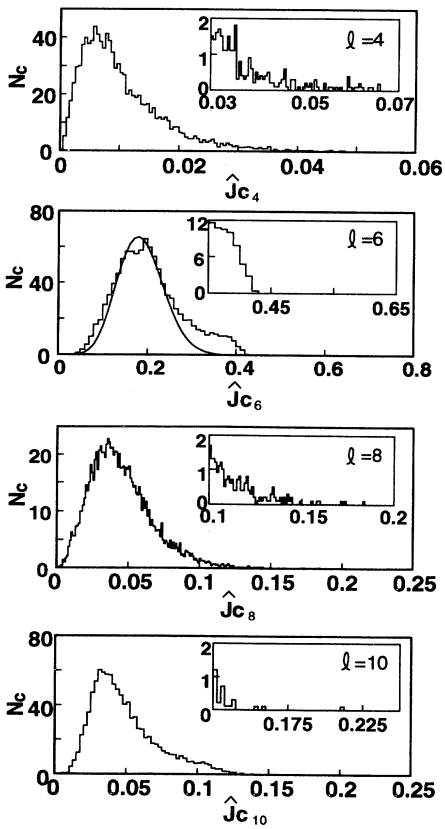

FIG. 10. Distributions of $\hat{J}c_l$ calculated for the model glass at 700 K (histogram, run D). The curve overlaid on the $\hat{J}_{c6}$ distribution shows the best fit of the main peak around a $\hat{J}_{c6}$ value of 0.18 with the six-dimensional Gaussian function.

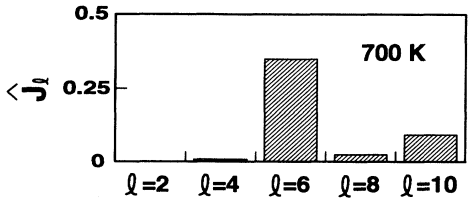

FIG. 11. $\hat{J}_l$'s calculated for the clusters with $\hat{J}_{c6}$ being larger than 0.3 in the model structure at 700 K (run D).

in the distribution is close to that for fcc clusters, 0.33. The clusters within the smaller peak, therefore, seem to correspond to the fcc or heavily deformed icosahedral type of clusters.

In order to identify the symmetry of the cluster within the smaller peak in the $\hat{J}c_6$ distribution, $\hat{J}_l$'s for the clusters of which $\hat{J}c_6$ is larger than 0.3 were calculated. Indeed the $\hat{J}_l$'s for such clusters were found to be very close to those of perfect icosahedra, as shown in Fig. 11 (see also Fig. 2 for comparison). From 10% to 12% of the clusters involved in the model glasses quenched to below T_g by our quenching procedures are of the icosahedral type as defined by $\hat{J}c_6$ being larger than 0.3. This number of the icosahedral clusters ($\hat{J}c_6 > 0.3$), $N_{\rm ics}$, increases when the system is relaxed below T_g as shown in Fig. 12. Note that, after an initial relaxation period of about 5×10^4 MD steps (5×10^{-11} sec), $N_{\rm ics}$ gradually increases and appears to be saturating to a value around 15% of the total number of the particles, which is close to the continuum percolation limit (about 0.15),[33] for various runs with different relaxation temperatures below T_g.

2. *Mirror-symmetric correlation among icosahedral clusters*

It is of great interest to see if there exists a strong orientational correlation among the icosahedral clusters.

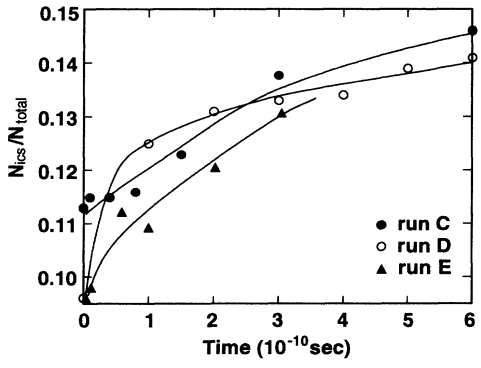

FIG. 12. Change in the number of the clusters with $\hat{J}_{c6}$ larger than 0.3, $N_{\rm ics}$, during structural relaxation. The relaxation temperature for the assemblies quenched by run C or D is 700 K, while that for the assembly by run E is 900 K.

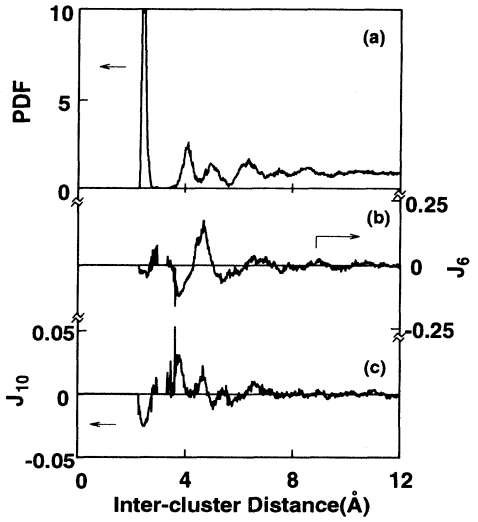

FIG. 13. (a) Partial pair distribution function of the atoms at the center of the icosahedral clusters with $\hat{J}_{c6}$ being more than 0.3, (b) $J_6(r)$, and (c) $J_{10}(r)$ for the icosahedral clusters in the model structure at 700 K (run A).

Thus we will, for a while, analyze the structure of the aggregates consisting of the clusters of which $\hat{J}c_6$ is larger than 0.3, rather than dealing with all clusters involved. Figure 13(a) shows the partial pair distribution function (PDF) for the central atoms of the icosahedral clusters. This partial PDF retains well the characteristics of glassy structures for which the second peak splits into two, and the positional correlation dies out at a large distance, but each peak is much sharper than in the total PDF.

Figures 13(b) and 13(c) display the partial $J_6(r)$ and $J_{10}(r)$ for the icosahedral clusters. The oscillatory behavior is again found in the functions. However, the first peaks in both $J_6(r)$ and $J_{10}(r)$ are negative unlike in those shown in Fig. 8. Moreover, the second peak is strongly negative for $J_6(r)$ and is positive for $J_{10}(r)$. It is noteworthy that the values of $J_6(r)$ and $J_{10}(r)$ for the peaks are very close to those deduced for the simple icosahedral aggregation shown in Table I. It is then natural to ask if the icosahedral aggregation possesses mirror symmetry at each interconnection and, if any, how far such correlation involving mirror symmetry extends. This type of correlation should be signified in the orientational correlation function $K_l(r)$ as a smoothly decaying curve as described previously. So as to calculate $K_l(r)$, the interconnection between the clusters, along which the mirror operation is performed by the operator R, must be defined explicitly.

Corresponding to the two interlocking states of icosahedra shown in Figs. 3(a) and 3(b), two kinds of interconnections between the icosahedral clusters can be defined. Since the two icosahedra in the interlocking state shown in Fig. 3(b) are nearest neighbors to each other, the simplest definition of interconnection between the clusters is that the distance between the clusters is less than 3.3 Å, which is equivalent to being within the first

peak in the partial PDF shown in Fig. 13. Let us call the percolation through this type of connectivity *α percolation,* which is approximated as a continuum percolation with a volume occupied by the atoms at the center of the icosahedral clusters, e.g., the total Voronoi volume[34] of the center atoms.

The simplest extension of the definition of connectivity is thus to define it to include both the first- and second-nearest icosahedral clusters, corresponding to the two interlocking states shown in Figs. 3(a) and 3(b). Thus we define the clusters also connected, when they are the second-nearest neighbors to each other and sharing three atoms on their vertices, which occurs in the interlocking state shown in Fig. 3(a). Most of the cluster pairs with the intercluster distance within the second peak in the PDF are in this topological situation. The second definition of connectivity is either when the distance between the clusters is less than 3.3 Å or the clusters share three atoms. We call the percolation through this type of connectivity *β percolation.*

Figure 14 illustrates an example of the interconnection network among the icosahedral clusters by β-percolation paths in our model glass below T_g. The volume of the icosahedral aggregates far exceeds the percolation limit for β percolation so that most of the cluster pairs have multiple connection paths. The volume ratio of the icosahedral clusters to the total space below T_g is estimated to be about 40% when the volume of the cluster is defined as the coordination polyhedron with an atom at the center and the nearest-neighbor atoms at its vertices (not the Voronoi polyhedron). Moreover, the number of the atoms which are located at either the center or vertices of the icosahedral clusters is approximately 80% of the total number of atoms below T_g. It is worth noting that triangular sites of the interconnection path, as frequently observed in Fig. 14, never cause the frustration of the mirror-operation processes, since an even number of the successive three-dimensional mirror operations does not necessarily rotate a cluster back to its initial orientation unless the mirror operations are those along the same direction unlike in the case of spins. Successive mirror operations of this type create an infinite variety of orientations of the clusters, and this is the reason for the complexity of this problem.

For evaluating $K_l(r)$, two more conditions as follows were set to eliminate the frustration on choosing a path among the multiple possible connection paths between the cluster pair as shown in Fig. 14.

(1) If there exist multiple connection paths between the cluster pair, the path consisting of the least number of the interconnections is taken.

(2) If there exist multiple connection paths consisting of the same least number of the interconnection units, the path with the least path length is taken; the path length is the sum of the length of the interconnections (sum of the length of the cluster bonds shown in Fig. 14).

Thus we analyze the percolation paths between the clusters with these definitions and then evaluate $K_l(r)$ involving the mirror operators. For instance, if the path between the ith and jth clusters is of $i \rightarrow o \rightarrow p \rightarrow j$, the mirror operator in Eq. (7) becomes $R_{io}R_{op}R_{pj}$.

We first evaluated $K_l(r)$'s along the extended connectivity, β-percolation paths, among the icosahedral clusters. The $K_l(r)$ scaled by $\hat{J}_l$ calculated along β-percolation paths for the model glass relaxed for 3×10^5 MD steps at 700 K is shown in Fig. 15. In this calculation, both interconnected and noninterconnected icosahedral cluster pairs are involved; when there is no

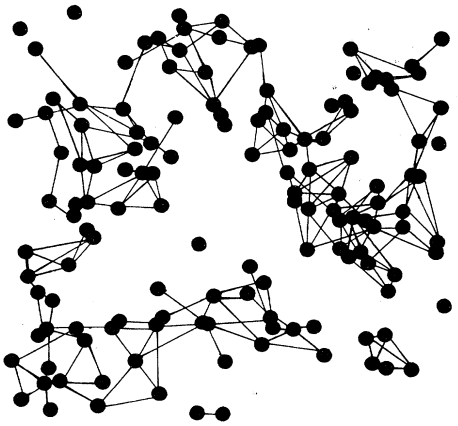

FIG. 14. Interconnection network among icosahedral clusters in the model structure at 700 K (see text for the definition). The solid circles represent the center atom of each icosahedral cluster (run A).

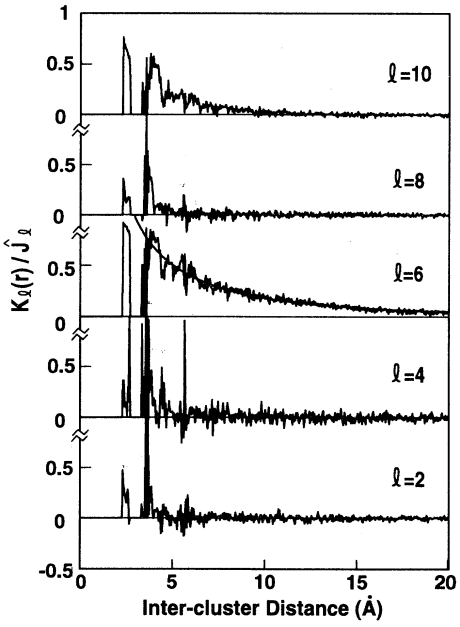

FIG. 15. $K_l(r)$'s calculated for the icosahedral aggregates in the model glass relaxed for 3×10^5 MD steps at 700 K (run D). The smooth curve overlaid on the $K_6(r)$ is the best fit with Onsager's formula.

path between a cluster pair, the mirror operator relevant to the cluster pair in Eq. (7) is defined to be 1, and therefore no mirror operation applied. The sharp valley existing at the cluster distance from 3 to 3.3 Å does not correspond to a sharp decrease in the orientational correlation, but is simply due to lack of cluster pairs existing at these distances (see the PDF in Fig. 13). Except for this unphysical valley, the $K_l(r)$'s are monotonically attenuating functions of r without such intense oscillation as appeared in $G_6(r)$ and $J_6(r)$, supporting the idea that the orientational relation between the clusters retains mirror symmetry. The mirror relation between the neighboring clusters is rather strong, since the $K_6(r)$ at r less than 4 Å is around 80% of $\hat{J}_6$, which is approximately the maximal possible value of $K_6(r)$. Beyond this distance, $K_6(r)$ and $K_{10}(r)$ attenuate gradually, while other functions of the second, fourth, or eighth order decay quickly and show almost no values at large distances; note that this selective behavior on the order l implies icosahedral symmetry. In particular, $K_6(r)$ exhibits a positive nonzero value even at 20 Å. This is rather surprising since the averaged number of the interconnection units lying on the path between the clusters of which the intercluster distance is 20 Å is more than 13. In other words, the successively mirrored angular correlation between the cluster pair survives even after 13 times of reflection operations.

Since the rate at which icosahedral clusters are interconnected by β-percolation paths below T_g is fairly large as shown in Fig. 14, the primary aspects of the $K_l(r)$'s seen in Fig. 15 are not altered whether the evaluation involves both interconnected and noninterconnected pairs or omits the latter. Indeed, for well-relaxed structures below T_g having many icosahedral clusters, both evaluation procedures give almost the same results. Moreover, the effect of quenching rates and structural relaxation on this evaluation is not significant. Although the above-mentioned positive tail of $K_6(r)$ becomes somewhat longer by decreasing quench rates or by relaxing model glasses when evaluating it with both interconnected and noninterconnected cluster pairs along β-percolation paths, the tail of $K_6(r)$ evaluated omitting noninterconnected pairs is hardly changed by such a thermal history. These facts suggest that although the density of icosahedral clusters is history dependent as shown in Fig. 12, the mirror-related orientational correlation along the interconnection paths is independent of thermal history. Relevant results calculated along β-percolation paths omitting noninterconnected cluster pairs will be presented later in Sec. IV D.

$K_l(r)$'s along α-percolation paths were then evaluated. For this calculation, noninterconnected icosahedral cluster pairs are neglected; the calculation without noninterconnected pairs provides us with information on not only the strength and length scale of the angular correlation, but also the maximal size of interconnected icosahedral aggregates, i.e., information on percolation. In Fig. 16, the $K_l(r)$'s calculated for the structure relaxed over 6×10^5 MD steps at 700 K are shown. Large fluctuations at large distances are statistical noise due to very small

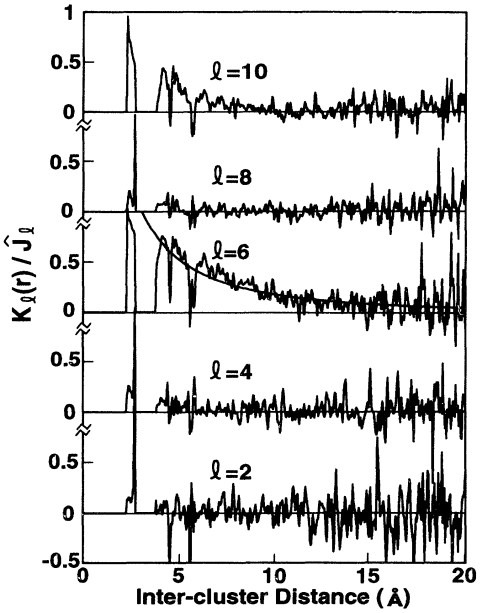

FIG. 16. $K_l(r)$'s evaluated along α-percolation paths in the structure relaxed for 6×10^5 MD steps at 700 K (run D). The smooth curve overlaid on the $K_6(r)$ is the best fit with Onsager's formula.

numbers of the interconnected icosahedral cluster pairs at the distance. Thus, as expected by the fact that the volume of the space occupied by the center atoms of the icosahedral clusters is just below the continuum percolation limit (see Fig. 12), α percolation appears to be nearly attained. Moreover, the sixth- and tenth-order functions evaluated along α-percolation paths exhibit a positive nonzero value up to large distances, although the correlation function of the second, fourth, or eighth order decays quickly and shows almost no signal beyond the distance of 4 Å. The selective behavior of the correlation functions on the order as well as the long positive tail of the sixth function agree well with those observed for the $K_l(r)$'s evaluated along β-percolation paths, indicating that the mirror-related orientational relation between neighboring icosahedral clusters is independent of the selection of paths and thus a rather universal property of the icosahedral aggregates in the glassy structure.

These $K_6(r)$'s can be fitted with Onsager's formula

$$a\frac{\exp(-r/\lambda)}{r}\ , \tag{8}$$

as shown in Figs. 15 and 16. The correlation length parameter λ, determined by fitting the particular $K_6(r)$ shown in Fig. 15 with this function, is 15 Å, and that for the $K_6(r)$ shown in Fig. 16 is also over 10 Å. As mentioned above, the positive tail of $K_6(r)$ depends on the thermal history of the model glass. For example, when the model glass is not well relaxed (just after our quenching procedures), the length scale parameter λ for fitting the $K_6(r)$ evaluated including both interconnected and noninterconnected cluster pairs along β-percolation paths

is from 5 to 10 Å, and it tends to increase to over 10 Å by structural relaxation below T_g. However, when evaluating $K_6(r)$ without noninterconnected cluster pairs, this fitting of the function with Onsager's formula almost always gives a value of λ over 10 Å, being independent of thermal history as well as the type of percolation path. Thus, among the clusters specified by $\hat{J}_6$ being larger than 0.3, a strong orientational correlation due to the nearest-neighbor anticorrelation always exists. The length scale of the correlation extends up to more than 5 times the contact interatomic distance in our model glasses.

So far we have investigated the successively mirrored orientational correlation only among the icosahedral clusters, since this concept has been introduced based upon a geometrical consideration of interlocking icosahedra. We now check here if this mirror-based orientational correlation between adjacent clusters is a universal property of the glassy structure irrespective of the topology of clusters. Although the evaluation of $K_6(r)$ along percolation paths as shown above is not directly applicable to an entire system involving all clusters because of an enormous number of percolation paths between clusters, the universality of the reflection-related orientational correlation can be investigated by the function

$$L_6(r)=\frac{1}{13}\frac{\sum_m \sum_{i,j} q_6{}^m(\vec{r}_i)R_{ij}q^{*m}_6(\vec{r}_j)\delta(|\vec{r}_i-\vec{r}_j|-r)}{\sum_{i,j} q_0{}^0(\vec{r}_i)q^{*0}_0(\vec{r}_j)\delta(|\vec{r}_i-\vec{r}_j|-r)} . \quad (9)$$

The term evaluating the orientational correlation in the numerator of this function involves only one mirror operator R for all the cluster pairs, which simply reflects the coordinates of a cluster of a pair along the bonds connecting the pair. Thus, whereas this function would not describe the mirror-related orientational correlation between the clusters that are the third-nearest neighbors to each other or beyond, if the orientational relation between adjacent clusters is strongly mirror related, it would result in large positive values at the distances of, perhaps, the first- and second-nearest neighbors. Figure 17 displays the $L_6(r)$ evaluated for the model structure at 700 K without averaging out thermal vibrations of atoms. It is seen that the function indeed exhibits large positive values at distances less than 5 Å, i.e., the first- and second-nearest-neighbor distances, and decays abruptly beyond this distance. This behavior should be compared with that of the $J_6(r)$ for the structure below T_g shown in Fig. 8. The value of the first peak in the $L_6(r)$ is approximately twice the value of the first peak in the $J_6(r)$. Furthermore, the second peak of the $L_6(r)$ is approximately 3 times larger in magnitude than that of the $J_6(r)$, and they possess different signs. Therefore, although the orientational correlation may be the largest among the icosahedral clusters, that between adjacent clusters can basically be described as the mirror-related orientational correlation irrespective of the topology of clusters.

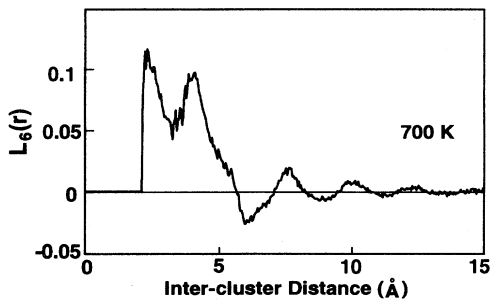

FIG. 17. $L_6(r)$ calculated for all the local clusters in the model glasses at 700 K using instantaneous positions of atoms (run A).

D. Temperature dependence of the orientational order

The temperature dependence of the symmetry coefficients of the local clusters, $\hat{J}_l$'s, is seen in Fig. 18. In this figure, the $\hat{J}_l$'s calculated using the instantaneous particle positions for run A are plotted as a function of temperature. At high temperatures, the dependence is linear, but deviations from the linearity occur at lower temperatures analogously to the behavior of pressure. However, except $\hat{J}_2$, the deviation from linearity occurs, well above T_g, around 1600 K, and then, at T_g, the temperature dependence changes again and becomes linear again at low temperatures. Let us call this upper transition temperature T_{g2}. It is noteworthy that T_{g2} is very close to the temperature below which spatial correlations

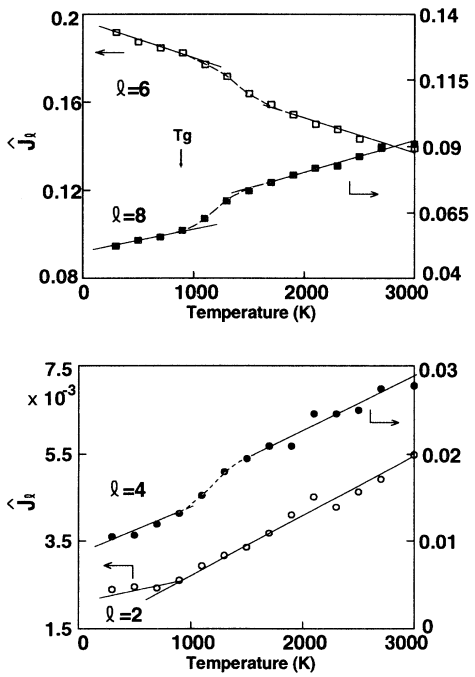

FIG. 18. Temperature dependence of the symmetry coefficients of the local clusters, $\hat{J}_l$'s, for run A.

between atomic shear stresses have been reported to develop in MD supercooled liquids using the same potential.[31] Moreover, among the symmetry parameters shown in Fig. 18, only the sixth-order parameter increases with decreasing temperature, whereas the others decrease. This trend implies that the clusters with icosahedral symmetry, which possess the lowest-order spherical harmonic component at $l=6$,[11] become more abundant at low temperatures, in particular below T_{g2}.

To investigate the temperature dependence of the topology of the local clusters further, the cluster symmetry coefficient for each cluster, $\hat{J}_{c6}$, was evaluated for the model structures at various temperatures. In Fig. 19 are the results shown as a temperature dependence of the distribution of the parameter among the clusters. At 1900 K, $\hat{J}_{c6}$ exhibits a simple higher-dimensional Gaussian-type distribution with a maximal distribution at the parameter value around 0.18. However, when the temperature is lowered through T_{g2}, a small peak appears around the parameter value of 0.35. The height of this small peak increases with decreasing temperature, and the increase then slows down below T_g. As stated previously and shown in Fig. 20, the clusters within this range possess strong icosahedral characteristics. The symmetry parameters $\hat{J}_l$'s of the clusters with $\hat{J}_{c6}$ larger than 0.3 are very close to those of an icosahedron irrespective of temperature, confirming that the anomalous temperature dependence of $\hat{J}_l$'s is caused by the increased density of the slightly distorted icosahedral clusters at low temperatures.

Figure 21 shows the number of the icosahedral clusters

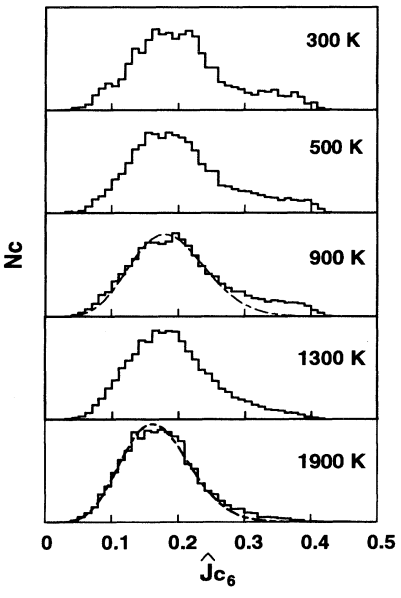

FIG. 19. Temperature dependence of the distribution of the symmetry coefficient $\hat{J}_{c6}$ (run A). The dashed lines show the best fit of the main peak around a $\hat{J}_{c6}$ value of 0.18 with the six-dimensional Gaussian function.

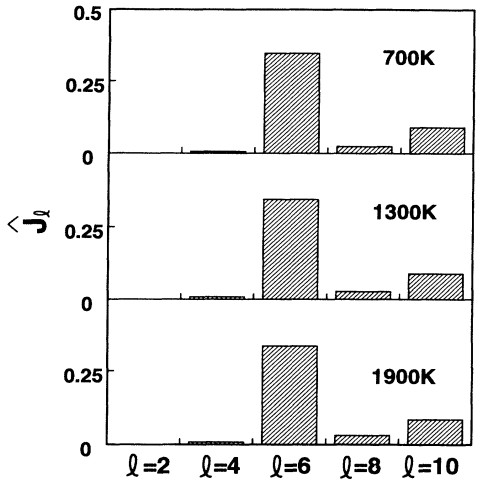

FIG. 20. $\hat{J}_l$'s for the clusters of which $\hat{J}_{c6}$ is more than 0.3 (run D).

with the $\hat{J}_{c6}$ value larger than 0.3, $N_{\rm ics}$ plotted against temperature. This temperature dependence illustrates well the rapid development of the above-mentioned subpeak in the $\hat{J}_{c6}$ distribution when lowering temperature from above T_{g2} and the sudden arrest of the increase at T_g. As temperature drops through T_{g2} and approaches T_g, the rate of increase in $N_{\rm ics}$ becomes higher, and the increase freezes when $N_{\rm ics}$ reaches a value of around 12% of the number of particles included in the system. In this figure, $N_{\rm ics}$'s at 1900 K calculated using atomic positions averaged for 0, 100, 1000, and 2000 MD time steps are also shown, in order to see how thermal vibrations and a large atomic diffusion at high temperatures affect the results. The $N_{\rm ics}$ is seen to be constant and maximal at the averaging period from 600 to 1000 MD steps. This dependence of $N_{\rm ics}$ on the number of MD steps tells us

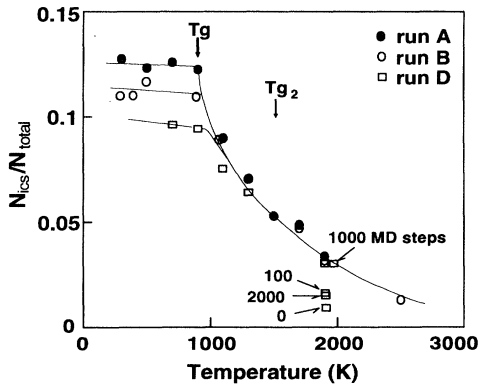

FIG. 21. Ratio of the number of the clusters with a $\hat{J}_{c6}$ value of more than 0.3, $N_{\rm ics}$, to the total number of the clusters in the system, $N_{\rm total}$, plotted against temperature.

that the effect of thermal vibration is adequately eliminated by averaging atomic positions for 600 MD steps, but diffusion limits the lifetime of the icosahedral clusters at 1900 K to be around 10^{-12} sec (1000 MD steps). It is worth noting that, as mentioned previously, even though the temperature dependence of pressure suggests a slightly higher transition temperature for run A than for the other runs (see Fig. 5), the freezing of the evolution shown in Fig. 21 marks approximately the same transition temperature around 900 K for any run in our simulation, showing that this structural change is a rather universal measure of freezing. Moreover, the value at which the evolution of $N_{\rm ics}$ is frozen depends weakly on quenching procedures, and $N_{\rm ics}$ increases, approaching a certain fixed range of values during a structural relaxation below 900 K, as has been shown in Fig. 12. This saturating variation of $N_{\rm ics}$ during relaxation below 900 K implies that the freezing temperature for $N_{\rm ics}$ would not be significantly lowered by such structural relaxation, although we have not investigated the effects of the relaxation on this freezing temperature because of a high crystallization rate above T_g.

In order to gain insight into the orientational correlation in the icosahedral aggregates developing in supercooled liquids, the successively mirrored orientational correlation functions $K_l(r)$ were again evaluated for the icosahedral clusters with a $\hat{J}_{c6}$ value larger than 0.3 at various temperatures.

$K_6(r)$ along β-percolation paths have been evaluated, and the results are shown in Figs. 22 and 23. In Fig. 22, the temperature dependence of the sixth-order function, scaled by $\hat{J}_6$, calculated neglecting the icosahedral cluster pairs without any interconnection path is shown. Below T_g, this correlation function exhibits a large value of about 70% of $\hat{J}_6$ at a distance of around 2.5 Å and decays slowly at a large distance, retaining a small but positive value even beyond the distance of 15 Å. At higher temperatures, although the variation at relatively short distances is almost the same as that below T_g, the function exhibits noisy behavior or a sharp cutoff at a large distance. This is due to a small number or an absence of interconnected cluster pairs at the distance. Thus, at 1900 K, the maximum size of the icosahedral aggregates interconnected by the β-percolation paths is about 15 Å, and β percolation is observed to have already been attained in the structure below 1300 K. The threshold temperature for β percolation is expected to lie around T_{g2}. In other words, there exists a strong successively mirrored orientational correlation in the icosahedral aggregates along β-percolation paths irrespective of temperature, and the icosahedral aggregates start to percolate with the connectivity throughout the liquid at a temperature close to T_{g2}. It is worth noting that the value of $K_6(r)$ at large distances at higher temperatures is somewhat larger than that below T_g. This behavior suggests that multiple connection paths between the icosahedral clusters due to large aggregation of the clusters at low temperatures impose a significant frustration on the successively mirrored orientational ordering, while the small aggregates are independent of each other; thus, the ordering is less frustrated in high-temperature liquids.

To account for both the successively mirrored orientational correlation along β-percolation paths and the rate at which the interconnection path is found between a cluster pair at a distance, we also calculated $K_6(r)$ involving both interconnected and noninterconnected

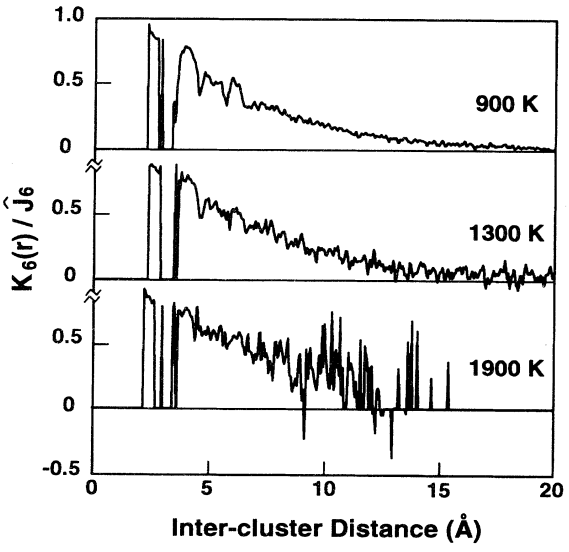

FIG. 22. $K_6(r)$ evaluated along β-percolation paths in the structures at various temperatures (run D). The evaluation was performed neglecting the icosahedral cluster pairs without any interconnection path.

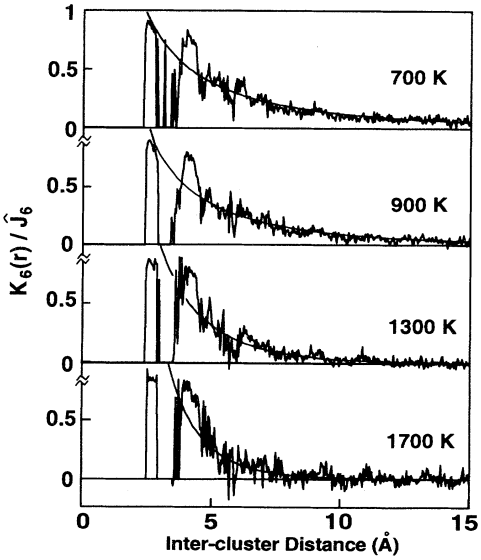

FIG. 23. $K_6(r)$ evaluated involving both interconnected and noninterconnected icosahedral cluster pairs along β-percolation paths in the structure at various temperatures (run A). The smooth curves are the best fit with Onsager's formula.

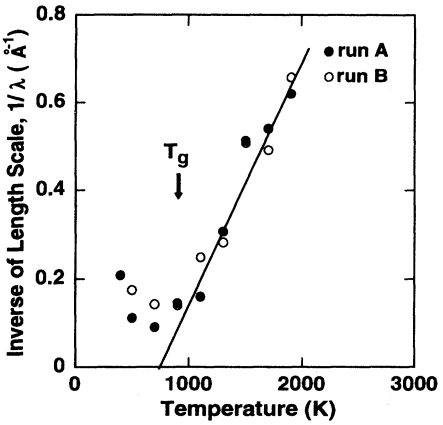

FIG. 24. Temperature dependence of the correlation length parameter λ for $K_6(r)$ evaluated involving both interconnected and noninterconnected icosahedral cluster pairs along β-percolation paths.

icosahedral cluster pairs by β-percolation paths. In this calculation, the mirror operators R relevant to the noninterconnected cluster pairs are neglected so that $K_l(r)$ becomes equal to $J_l(r)$ when no interconnected pair exists at the distance of r (the same procedure as that used for the calculation shown in Fig. 15). Typical examples of the results are shown in Fig. 23. At low temperatures below T_g, this $K_6(r)$ is almost the same as that calculated neglecting noninterconnected cluster pairs, reassuring that most of the icosahedral clusters are interconnected at distances within our simulation box. At high temperatures, $K_6(r)$ decays rapidly at distances beyond 5 Å. Thus the existence probability of the interconnection path at high temperatures attenuates quickly at distances beyond 5 Å, while the maximum size of the icosahedral aggregates is 15 Å even at 1900 K. It is also suggested that the orientational correlation that may appear in $J_6(r)$ does not exist between the noninterconnected icosahedral cluster pair. These correlation functions at high temperatures can also be fitted by Onsager's formula as shown by the smooth solid lines in Fig. 23. Figure 24 displays the temperature dependence of the correlation length parameter λ for fitting those $K_6(r)$'s. As the temperature drops from a high temperature through T_{g2}, λ increases markedly, and then this increase freezes below T_g. It is also interesting to note that, above T_g, this length scale varies as a function of temperature, $b/(T-T')$, at temperatures above T_g, where T' is a temperature slightly below T_g and b is a constant.

V. DISCUSSION

Since the configuration of the atom in the first coordination cell around a central atom prefers icosahedral symmetry, as stated by Frank,[10] it is not surprising at all that our model glasses have involved many local clusters of the icosahedral type. Indeed, such clusters have been observed in previous intense studies on the topology of local atomic configurations in glasses.[9] However, importantly, the number of the local clusters of an icosahedral type increases rapidly when temperature is decreased, and then this increase freezes at T_g. In this process, the volume of the space occupied by the icosahedral clusters reaches a threshold value, at which β percolation is attained, at a temperature of about 500 K above T_g. Then, at T_g, the aggregation of the icosahedral clusters is arrested just before the volume reaches the limit for α percolation. Furthermore, in the icosahedral aggregates there exists a successively mirrored orientational order with a length scale of about 10 Å.

A. Bimodal structure

As stated previously, a four-dimensional sphere completely filled by icosahedra alone can be used as a template for glassy structures in real flat space. The real structure is then produced by introducing appropriate disclinations into the four-dimensional structure such that mapping onto flat space can be performed.[1] In this framework, the icosahedral aggregates observed in our model glasses could be regarded as the part left intact during the mapping process and the rest of the structure as the part disclinated. Since the undisclinated region in our model glasses below T_g involves approximately 80% of the total atoms when counting both the centered atoms and the ones at the vertices of the icosahedral clusters, the glassy structure can be viewed as an icosahedral aggregate surrounded by a highly localized disclination network, therefore a bimodal structure.

This bimodal structure possesses similarity to glass or liquid structures proposed in the free-volume theory by Cohen and co-workers[20–22] and in the "significant structure" theory by Eyring and Jhon.[35] In these theories, the authors also assumed a bimodal structure where solidlike and liquidlike regions coexist. The free-volume theory then interprets the glass transition as a manifestation of the percolation of the liquidlike part involving excess space, i.e., the free volume, which contributes to the diffusion of atoms. Since the local icosahedral arrangement of atoms is one of the densest local packing, the part consisting of the icosahedral aggregates in our model structure can be regarded as the solidlike region in the theories, and the rest of the structure as the liquidlike one. Our observation suggests the presence of the mirror-symmetric orientational order of an extended length scale in the solidlike region, whereas these theories are only phenomenological. In our view the recently developed mode-coupling theory should be revised, since the theory assumes the structure of supercooled liquids to be homogeneous and to possess only local order confined within the scale of atoms, while in the present work the two types of domains and the extended orientational order were observed below T_{g2}. Therefore the mode-coupling theory in the present form may not be valid below T_{g2}.[31]

The observed bimodal structure here may also be relevant to nanoscale inhomogeneities or medium-range orders[36–40] that have been suggested experimentally for various network glasses. For example the low-frequency peak of Raman spectra[36,37] as well as other vibrational

properties observed by infrared or light scattering measurements[38,39] for these glasses have been ascribed by many authors to some granularities (fluctuations in density or chemical compositions) or structural correlations on a length scale from 10 to 20 Å. Although the nature of the bonding between atoms, and thus the nature of local atomic configurations, is much different in the network glasses from our simple system with a spherically symmetric interatomic potential, it may still be possible that such a structural correlation is understood within the framework described above, i.e., the bimodal structure involving the orientational correlation with some necessary modifications.

B. Orientational freezing (tensorial glasses)

Although Steinhardt, Nelson, and Ronchetti[11] claimed to have identified the "ferromagnetic" ordering of the local BOO tensor $q_6{}^m$ in their Lennard-Jones MD glasses, the present results indicate that the order is not ferromagnetic but of "antiferromagnetic" type. This is because two interlocking icosahedral clusters have opposite signs of $q_6{}^m$. This $q_6{}^m(r_i)q^*{}_6{}^m(r_j)$ becomes negative for the interlocking state as shown in Table I, and the interlocking state was abundantly observed in the model glasses. Thus the simple effective Hamiltonian may be written as

$$H=-J\sum_{\langle i,j\rangle}\sum_{m=-6}^{6} q_6{}^m(\vec{r}_i)q^*{}_6{}^m(\vec{r}_j)\ , \tag{10}$$

where the interaction parameter J is not positive but negative and the symbol $\langle i,j\rangle$ denotes a sum over pairs of nearest neighbors. In reality J is not a constant, but in the simplified model Hamiltonian we could regard it as a constant. More precisely, since the orientational relation between the interlocking icosahedral clusters is best described by the mirror symmetry, the Hamiltonian may need to be modified using the mirror operator R as follows:

$$H=-J\sum_{\langle i,j\rangle}\sum_{m=-6}^{6} q_6{}^m(\vec{r}_i)R_{ij}q^*{}_6{}^m(\vec{r}_j)\quad (J>0)\ . \tag{11}$$

The mean-field theory after Haymet[41] using the former Hamiltonian predicts that the positive J gives rise to the first-order transition to the "ferromagnetically" ordered states at a low temperature.

However, the Hamiltonian in Eq. (10) with negative J or the latter Hamiltonian will most likely lead to a spin-glass-like state at low temperatures. The negative interaction or mirror-symmetric correlation between clusters would produce a significant frustration on the alignment of the clusters in spatially disordered systems as in real spin-glass systems. As a result, the local BOO tensor $q_6{}^m$ would be frozen in relatively random directions, and the correlation length of the orientational order described by $K_6(r)$ will never become infinite, but will be frozen at a medium distance as observed here. In this way, the structure of glasses is best described not as a spin glass, but as a tensorial glass, and the glass transition could be the manifestation of a transition from a spherically symmetric liquid to a tensorial glass.

C. Energy states of the icosahedral clusters

In liquids and glasses, the energy of local clusters varies from one site to another depending on their own geometry and environment. If there exists a geometrical state of the cluster of which the energy is significantly lower than other states, the clusters with such a geometry should dominate at low temperatures. Conversely, at the high-temperature limit, all the geometrical states would be activated equally by thermal excitation. Consequently, the distribution of the cluster geometry should be directly connected with the distribution of states, for instance, in a geometry parameter space. Thus, from the distribution of the cluster-symmetry coefficient $\hat{J}_{c6}$ observed at temperatures well above T_{g2} (e.g., the bottom histogram in Fig. 19), it is seen that, at high temperatures, only a small portion of the clusters is distributed in a $\hat{J}_{c6}$ range of more than 0.3, i.e., the range corresponding to the icosahedral clusters. Furthermore, the distribution of nonicosahedral clusters in $\hat{J}_{c6}$ space hardly changes when decreasing the temperature, while the number of the icosahedral cluster does increase significantly. This behavior suggests that the energy difference among the nonicosahedral clusters is small compared to that between the nonicosahedral and icosahedral ones. These considerations lead to a simple picture on the energy states of the clusters as shown in Fig. 25, in which the nonicosahedral topological states form a relatively narrow energy band, while the icosahedral states lie at lower-energy levels.

Let us estimate here the energy difference between the nonicosahedral and icosahedral states, E_b. Since, at temperatures above T_{g2}, β percolation is not yet attained and the clusters are thought to be effectively almost uncorrelated to each other, the icosahedral cluster could appear at any site in the system with the same probability and therefore complete mixing of the icosahedral clusters is

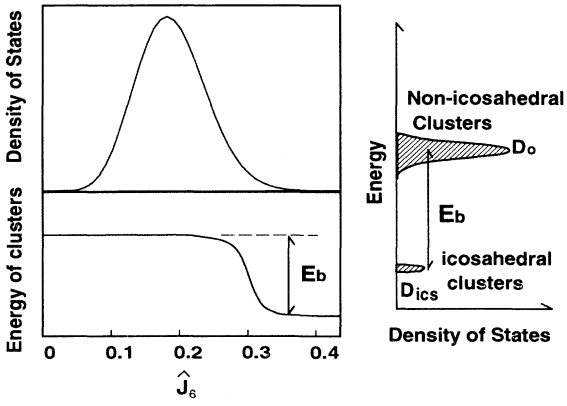

FIG. 25. Schematic representation of energy states of the local clusters.

obtained. The entropy associated with the complete mixing or distribution of the icosahedral clusters is written as

$$S = k_B \ln P = k_B \ln \left[\frac{N_{\text{total}}!}{(N_{\text{total}} - N_{\text{ics}})! N_{\text{ics}}!} \right] , \tag{12}$$

P being the number of distinguishable arrangements. Thus ΔG associated with the N_{ics} formation of the icosahedral clusters is given by

$$\Delta G = N_{\text{ics}}(\Delta H' - T\Delta S') - k_B T \ln \left[\frac{N_{\text{total}}!}{(N_{\text{total}} - N_{\text{ics}})! N_{\text{ics}}!} \right] , \tag{13}$$

where $\Delta H'$ and $\Delta S'$ denote the enthalpy and entropy differences between the icosahedral and nonicosahedral topological states, respectively. The equilibrium number of the icosahedral clusters is then determined by the equation

$$\frac{d\Delta G}{dN_{\text{ics}}} = 0 . \tag{14}$$

By using Stirling's theorem, we obtain the following equation for N_{ics} at equilibrium:

$$N_{\text{ics}} = \frac{N_{\text{total}}}{1 + \exp[(\Delta H' - T\Delta S')/k_B T]} . \tag{15}$$

This distribution law is equivalent to that used in a two-state model[42] or the bond-lattice model[43,44] for describing the thermodynamic properties of network glasses and the glass transition.

In our model in constant volume,

$$\Delta H' = E_b , \tag{16}$$

and $\Delta S'$, which represents the difference in degeneracy of the two states, the icosahedral and nonicosahedral states, is given by

$$\Delta S' = k_B \ln \left[\frac{D_{\text{ics}}}{D_0} \right] . \tag{17}$$

Here D_{ics} and D_0 represent the degeneracies of the icosahedral and nonicosahedral states or the densities of states at the correspondent two energy levels shown in Fig. 25, respectively. Putting Eqs. (16) and (17) into Eq. (15) then yields the equation determining the equilibrium number of the icosahedral clusters under the zeroth-order approximation of the energy state on the topology of the cluster shown in Fig. 25,

$$N_{\text{ics}} = \frac{N_{\text{total}} D_{\text{ics}} \exp(-E_b/k_B T)}{D_{\text{ics}} \exp(-E_b/k_B T) + D_0} . \tag{18}$$

Since, as mentioned previously, $D_{\text{ics}} \ll D_0$ and the term $\exp(-E_b/K_b T)$ would not be very large at temperatures above T_{g2}, the above equation is approximated as

$$N_{\text{ics}} \simeq \frac{N_{\text{total}} D_{\text{ics}} \exp(-E_b/k_B T)}{D_0} . \tag{19}$$

By fitting the observed temperature dependence of N_{ics} at temperatures above T_g with Eq. (19), we obtain $-E_b/k_B$ of about 7000 K for our system, as shown in Fig. 26; D_0/D_{ics} for this fitting is about 1250, justifying $D_{\text{ics}} \ll D_0$. Note that this value of $|E_b|$ is close to the energy difference between icosahedral and cuboctahedral clusters, about $5k_B T_m$, calculated by Frank[10] and Haymet[41] for the particles interacting with inverse power potentials, where T_m is the melting point of the systems ($5T_m$ of our system is approximately 9000 K). Although their calculations are not for the clusters surrounded by others, but for the clusters in isolation, this agreement supports the above simple picture of the energy states of the cluster in the high-temperature regime.

When the temperature drops below T_{g2}, the local clusters in liquids start being correlated. A simple effective Hamiltonian initiating this order may be described by Eq. (11), as stated above. This interaction is larger among the icosahedral clusters, since they possess larger $q_6{}^m$ components than the nonicosahedral clusters, and restrict the orientation and topology of a cluster next to another cluster. Among the nonicosahedral clusters, this restriction on the geometry of the clusters would be smeared out since the nonicosahedral clusters are within a small energy band and therefore the adjacent clusters can change their geometry almost without energy cost. However, because of the interaction above when an icosahedral cluster appears adjacent to another icosahedral cluster, the orientations of the two are likely to be strongly correlated. Since the reorientation of an icosahedral cluster would need to break up itself once and to reform an icosahedral cluster with other orientations, which requires to overcome an energy barrier of $|E_b|$ (about 0.7 eV as estimated above), most of the other orientational states for the cluster would not be accessible. The more the icosahedral aggregation develops, the larger the barrier height becomes because the reorientation of the large

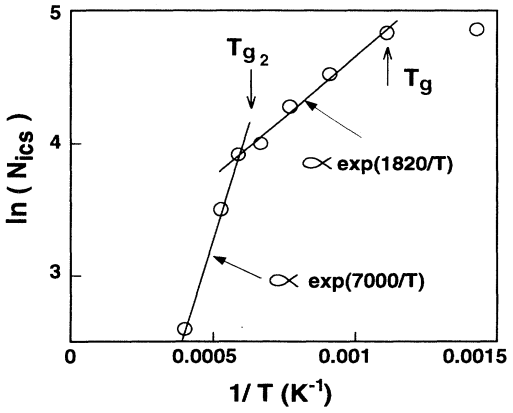

FIG. 26. Arrhenius plot of the number of the icosahedral clusters. Note that a sharp slope change appearing to exist at T_{g2} is presumably due to a statistical uncertainty of the data. The slope is likely to change gradually in a certain temperature interval around T_{g2}.

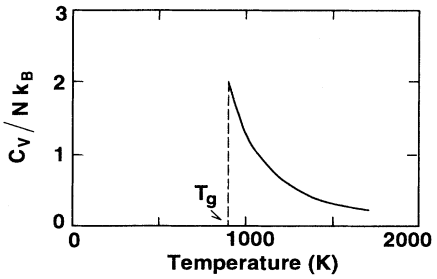

FIG. 27. Estimated specific heat change due to forming the icosahedral clusters.

icosahedral aggregates obviously needs simultaneous breakup of many icosahedral clusters. This gradual freezing out of the degree of freedom is perhaps the reason for the departure from the $\exp(-E_b/k_BT)$ type temperature dependence of the number of the icosahedral clusters occurring below T_{g2} shown in Fig. 26.

The simple picture on the thermodynamics of the clusters above thus breaks down below T_{g2}. Nevertheless, it is still tempting to estimate the energy gain due to forming icosahedral clusters above T_g, assuming that the energy gain is $\rho_{\rm ics}|E_b|$. Approximating the temperature dependence of $\rho_{\rm ics}$ in the temperature range between T_g and T_{g2} as another exponential function of $-E_c/k_BT$ ($|E_c|<|E_b|$, see Fig. 26), the energy gain of our system due to the formation of the icosahedral clusters is obtained to be

$$0.0115 \exp\left[\frac{1820}{T}\right] \text{(eV/atom)}, \tag{20}$$

where T is the temperature in kelvin. This energy gain gives the value of 0.087 eV/atom at T_g. The contribution of the energy gain to the specific heat is then

$$2.1\times10^5 \frac{\exp(1820/T)}{T^2} Nk_B , \tag{21}$$

where N is the number of atoms. As displayed in Fig. 27, this contribution of forming the icosahedral clusters to the specific heat is equal to about $2Nk_B$ at T_g and would be sharply reduced when the temperature is lowered below T_g because of the structural arrest occurring at the temperature (i.e., $\partial\rho_{\rm ics}/\partial T\rightarrow 0$). This temperature dependence of the specific heat is comparable to that of our system deduced from the total energy variation above T_g shown in Fig. 6. Although the above estimate should not be directly compared with experimental data since our calculation is in the constant-volume mode, it is noteworthy that the estimated specific heat variation well reproduces the salient characteristics of the specific heat change observed in real experiments.[45]

D. Percolation and viscous liquids

We now consider here some implications of the successively mirrored orientational correlation and the percolation on the properties of supercooled liquids and the glass transition. As mentioned previously, T_{g2}, around which β percolation is attained, is close to the temperature below which atomic shear stress correlations have been reported to develop in supercooled liquids by MD using the same potential.[31] In this study of the stress correlations, it has also been shown that a significant density of shear phonons can be supported in the temperature range between T_g and the characteristic temperature much above T_g. These behaviors of the stress correlation and vibrational density of states could simply be a consequence of β percolation. Since the icosahedral clusters are considered to be at a significantly lower-energy level than the clusters with other geometries, the icosahedral clusters would survive a breakup by thermal activation for a much longer time. Indeed, the lifetime of the icosahedral clusters at 1900 K, much above T_{g2}, has been observed to be around 10^{-12} sec in our simulation, which is approximately 5 times the period of the transverse phonon at its maximal density of states.[31] Moreover, a considerable successively mirrored orientational correlation exists among the icosahedral clusters even at a high temperature. It is thus conceivable that when β percolation is achieved at T_{g2} the percolating icosahedral aggregates start mediating, in part, long-range stress fields and lead to the observation of partial propagation of shear phonons.

In this viscous liquid in the temperature range between T_g and T_{g2}, atoms can still rearrange themselves in response to a temperature decrease so that the configuration accommodates more of the icosahedral clusters during cooling. The glass transition is marked by the sudden arrest of the reconfiguration as well as the rapid change in many other properties. However, the change in the structure from a liquid to a glass takes place gradually over the temperature interval between T_{g2} and T_g. As shown in Fig. 27, excess specific heat is observed over this range, implying freezing of configurational entropy. This gradual freeze-in of configurational entropy above the glass transition is very similar to that of a spin glass. Indeed, the effective Hamiltonian in Eq. (10) is similar to the exchange Hamiltonian for a spin glass, except that the local operators are tensors rather than vectors, and that the coefficients are likely to be temperature dependent,[46] while at this moment it is not possible to determine the explicit temperature dependence of these effective parameters.

At the same time it is possible to make a connection to the phenomenological theory of Saslow[27] in which the VTF law is derived by a Landau theory assuming the frustration between the local order and the global order. Our local bond orientational order parameter $q_l^m(r_i)$ may be used directly as the local variable in this theory. Below T_{g2} dynamic correlations among the q's, or the successively mirrored orientational correlations of icosahedral clusters, start to develop, but it will soon encounter frustration and the dynamics will slow down, leading to a glass transition at T_g.

The present simulation was carried out using a short-range potential and keeping the volume of the system constant under a periodic boundary condition. The use

of the long-range potential may influence the orientational correlations, but it is not likely to alter the nature of the correlations and their temperature dependence. The effects of keeping the volume constant and the periodic boundary conditions are more difficult to assess, but the fact that several models with somewhat different densities and different periodicities of the boundary showed practically identical results suggests that the effects would not be important. Nevertheless, this point deserves further investigations using a constant-pressure method.

VI. CONCLUSIONS

The orientational order in supercooled liquids was studied by geometrical considerations based on the spherical harmonic representations of the orientation of the bonds and clusters and the molecular dynamics simulations of the monatomic model supercooled liquids with the modified Johnson potential. In this study, the concept of the successively mirrored correlation due to interlocking states of neighboring icosahedral clusters was introduced, and it was carefully investigated in the model structures.

Although our MD results showed no indication of the long-range icosahedral BOO reported by Steinhardt, Nelson, and Ronchetti,[11] the aggregation of the clusters of an icosahedral type and the associated successively mirrored orientational order were found to be the key to the understanding of the structure of liquids. The distribution of the $l=6$ spherical harmonic symmetry parameter of the local clusters exhibits a small subpeak which corresponds to the presence of the clusters with an icosahedral topology. The number of the local clusters with icosahedral characteristics in the symmetry coefficients increases rapidly during cooling from a high temperature, and then this increase is abruptly arrested at T_g. In the course of cooling, the volume of the space occupied by the icosahedral clusters reaches a threshold value, at which β percolation is attained, at a temperature much higher than T_g. Then, at T_g, aggregation of the icosahedral clusters is arrested just before the volume reaches the limit for α percolation. α percolation can be approximated as the continuum percolation of the volume occupied by center atoms of the icosahedral clusters, while β percolation is a more extended one involving the connectivity between the clusters that are first- or second-nearest neighbors to each other. It has been further shown that the successively mirrored orientational correlation with a length scale over 10 Å exists along both types of percolation paths in the icosahedral aggregates. The estimated internal energy decrease due to the formation of the icosahedral clusters and its contribution to the specific heat reasonably match the energetic preference of icosahedral clusters stressed by Frank[10] and experimental specific heat changes above T_g, respectively. This extensive structural change above T_g associated with the orientational correlation over a relatively long length scale suggests a collective nature underlying the glass transition.

ACKNOWLEDGMENTS

The authors are grateful to Dr. E. Marshal and A. Seki for assisting in the computations. They also acknowledge the use of the facility of the Laboratory for Research on the Structure of Matter supported by the National Science Foundation through Grant No. DMR91-20668.

APPENDIX

The explicit expression of the modified Johnson potential in Ref. 29 is as follows: for $1.9 \le r \le 2.4$,

$$\phi(r) = -12.900\,21(r-2.4)^4 - 15.096\,18(r-2.4)^3 + 1.372\,738(r-2.4)^2 - 0.504\,774\,7(r-2.4) - 0.200\,210\,8 ;$$

for $2.4 \le r \le 3.0$,

$$\phi(r) = -0.639\,230(r-3.115\,829)^3 + 0.477\,871r - 1.581\,570 ;$$

for $3.0 \le r \le 3.44$,

$$\phi(r) = 14.671\,11(r-3.0)^5 - 12.910\,63(r-3.0)^4 + 1.725\,326(r-3.0)^3 + 0.222\,124\,1(r-3.0)^2 + 0.452\,142\,6(r-3.0) - 0.146\,963\,6 .$$

Here the potential ϕ and the distance r are in eV and Å, respectively.

[1] M. Kléman and J. F. Sadoc, J. Phys. (Paris) Lett. **40**, L569 (1979).
[2] J. F. Sadoc, J. Non-Cryst. Solids **44**, 1 (1981).
[3] M. Kléman, in *Continuum Models of Discrete Systems 4,* edited by O. Brulin and R. K. T. Hsieh (North-Holland, Amsterdam, 1981), pp. 287–296.
[4] D. R. Nelson, Phys. Rev. B **28**, 5515 (1983).
[5] S. Sachdev and D. R. Nelson, Phys. Rev. Lett. **53**, 1947 (1984).
[6] J. D. Bernal, Proc. R. Soc. London A **280**, 299 (1964).
[7] J. L. Finney, Proc. R. Soc. London A **319**, 479 (1970).
[8] J. D. Bernal and J. L. Finney, Discuss. Faraday Soc. **43**, 62 (1967).
[9] R. Yamamoto, H. Shibata, and M. Doyama, Phys. Status Solidi A **51**, 163 (1979).
[10] F. C. Frank, Proc. R. Soc. London A **215**, 43 (1952).
[11] P. J. Steinhardt, D. R. Nelson, and M. Ronchetti, Phys. Rev. Lett. **47**, 1297 (1981); Phys. Rev. B **28**, 784 (1983).
[12] R. M. Ernst and S. R. Nagel, Phys. Rev. B **34**, 8070 (1991).
[13] J. Jäckel, Rep. Prog. Phys. **49**, 171 (1986).
[14] W. Kauzmann, Chem. Rev. **43**, 219 (1948).
[15] H. Kui and D. Turnbull, J. Non-Cryst. Solids **94**, 62 (1991).
[16] R. Brüning and K. Samwer, Phys. Rev. B **46**, 11 318 (1992).
[17] J. O. Strom-Olsen, D. H. Ryan, and Z. Altounian, Mater. Sci. Eng. A **133**, 403 (1991).
[18] J. H. Gibbs and E. A. DiMarzio, J. Chem. Phys. **48**, 2560 (1958).

[19]G. Adam and J. H. Gibbs, J. Chem. Phys. **43**, 139 (1965).
[20]D. Turnbull and M. H. Cohen, J. Chem. Phys. **34**, 120 (1961).
[21]D. Turnbull and M. H. Cohen, J. Chem. Phys. **52**, 3038 (1970).
[22]M. H. Cohen and G. S. Grest, Phys. Rev. B **20**, 1077 (1979).
[23]E. Leutheusser, Phys. Rev. A **29**, 2765 (1984).
[24]E. Leutheusser, Phys. Rev. B **55**, 235 (1984).
[25]T. R. Kirkpatrick, Phys. Rev. A **31**, 939 (1985).
[26]U. Bengtzelius, W. Götze, and A. Sjölander, J. Phys. C **17**, 5915 (1984).
[27]W. M. Saslow, Phys. Rev. B **37**, 676 (1988).
[28]H. Vogel, Phys. Z **22**, 645 (1921); G. S. Fulcher, J. Am. Ceram. Soc. **8**, 339 (1925); G. Tamman and W. Hesse, Z. Anorg. Allg. Chem. **156**, 245 (1926).
[29]T. Egami and V. Vitek, in *Amorphous Materials,* edited by V. Vitek (TMS-AIME, Warrendale, PA, 1983), p. 127.
[30]R. A. Johnson, Phys. Rev. **134**, 1329 (1964).
[31]S.-P. Chen, T. Egami, and V. Vitek, Phys. Rev. B **37**, 2440 (1988).
[32]T. Egami and D. Srolovitz, J. Phys. F **12**, 2141 (1982).
[33]H. L. Fitzpatrick, R. B. Malt, and F. Spaepen, Phys. Lett. **47A**, 207 (1974).
[34]G. F. Voronoi, J. Reine Angrew. Math. **134**, 198 (1908).
[35]See, for instance, H. Eyring and M. S. Jhon, *Liquid Structures,* 1st ed. (Wiley, New York, 1969).
[36]E. Duval, A. Boukenter, and T. Achibat, J. Phys. Condens. Matter **2**, 10 227 (1990).
[37]A. P. Sokolov, A. Kisliuk, M. Soltwisch, and D. Quitmann, Phys. Rev. Lett. **69**, 1540 (1992).
[38]M. D. Ingram, G. D. Chryssikos, and E. I. Kamitsos, J. Non-Cryst. Solids **131-133**, 1089 (1991).
[39]C. T. Moynihan and J. Schroeder, J. Non-Cryst. Solids **160**, 52 (1993).
[40]P. H. Gaskell, M. C. Eckersley, A. C. Barnes, and P. Chieux, Nature **350**, 675 (1991).
[41]A. D. J. Haymet, Phys. Rev. B **27**, 1725 (1983).
[42]P. B. Macedo, W. Capps, and T. A. Litovitz, J. Chem. Phys. **44**, 3357 (1966).
[43]C. A. Angel and J. Wong, J. Chem. Phys. **53**, 2053 (1970).
[44]C. A. Angel and K. J. Rao, J. Chem. Phys. **57**, 470 (1972).
[45]H. S. Chen and D. Turnbull, J. Chem. Phys. **48**, 2560 (1968).
[46]T. Egami, T. Tomida, D. Kulp, and V. Vitek, J. Non-Cryst. Solids **156-158**, 63 (1993).